Letter | Editors' Suggestion

Colossal magnetoresistance via avoiding fully polarized magnetization in the ferrimagnetic insulator $Mn_3Si_2Te_6$

Yifei Ni,[1] Hengdi Zhao,[1] Yu Zhang,[1] Bing Hu,[1,2] Itamar Kimchi,[3] and Gang Cao[1,*]

[1]*Department of Physics, University of Colorado at Boulder, Boulder, Colorado 80309, USA*

[2]*School of Mathematics and Physics, North China Electric Power University, Beijing 102206, China*

[3]*School of Physics, Georgia Institute of Technology, Atlanta, Georgia 30332, USA*

(Received 31 December 2020; accepted 1 April 2021; published 14 April 2021)

Colossal magnetoresistance is of great fundamental and technological significance and exists mostly in the manganites and a few other materials. Here we report colossal magnetoresistance that is starkly different from that in all other materials. The stoichiometric $Mn_3Si_2Te_6$ is an insulator featuring a ferrimagnetic transition at 78 K. The resistivity drops by seven orders of magnitude with an applied magnetic field above 9 T, leading to an insulator-metal transition at up to 130 K. However, the colossal magnetoresistance occurs only when the magnetic field is applied along the magnetic hard axis and is surprisingly absent when the magnetic field is applied along the magnetic easy axis where magnetization is fully saturated. The anisotropy field separating the easy and hard axes is 13 T, unexpected for the Mn ions with nominally negligible orbital momentum and spin-orbit interactions. Double exchange and Jahn-Teller distortions that drive the hole-doped manganites do not exist in $Mn_3Si_2Te_6$. The phenomena fit no existing models, suggesting a unique, intriguing type of electrical transport.

DOI: 10.1103/PhysRevB.103.L161105

Colossal magnetoresistance (CMR) was first observed in the hole-doped perovskite manganites in the early 1990's. This discovery was followed by an explosion of interest in these materials. In the following decades, extensive efforts have resulted in comprehensive insights into the rich physics of this class of materials [1–16]. The hole-doped manganites, such as $La_{1-x}Ca_xMnO_3$, feature mixed oxidation states of Mn^{3+} and Mn^{4+}, a key element of this class of CMR materials. In essence, the concurrent magnetic and insulator-metal transitions in these materials arise from a combined effect of double exchange, which dictates magnetism, and Jahn-Teller distortions, which drive electrical transport [13–16]. An important exception was later found in the pyrochlore $Tl_2Mn_2O_7$ having the nominal oxidation state of Mn^{4+}, without double exchange and Jahn-Teller polarons [17]. This material undergoes a simultaneous ferromagnetic and insulator-metal transition at 135 K, resulting in CMR near the transition temperature [17]. A theoretical model developed for the pyrochlore manganite attributes the phenomena to magnetic polarons forming above the Curie temperature on the condition that the carrier density is sufficiently low [18]. This model is also used to explain CMR recently discovered in the antiferromagnetic $Eu_5In_2Sb_6$ [19]. Negative magnetoresistivity (MR) is also predicted in topological Weyl/Dirac semimetals, arising from the chiral anomaly $\vec{E}\cdot\vec{B}$ term, thus relying on an electrical current parallel to magnetic fields [20]. It has become increasingly clear that CMR, a phenomenon of great fundamental and technological significance, is far from being fully explored and understood.

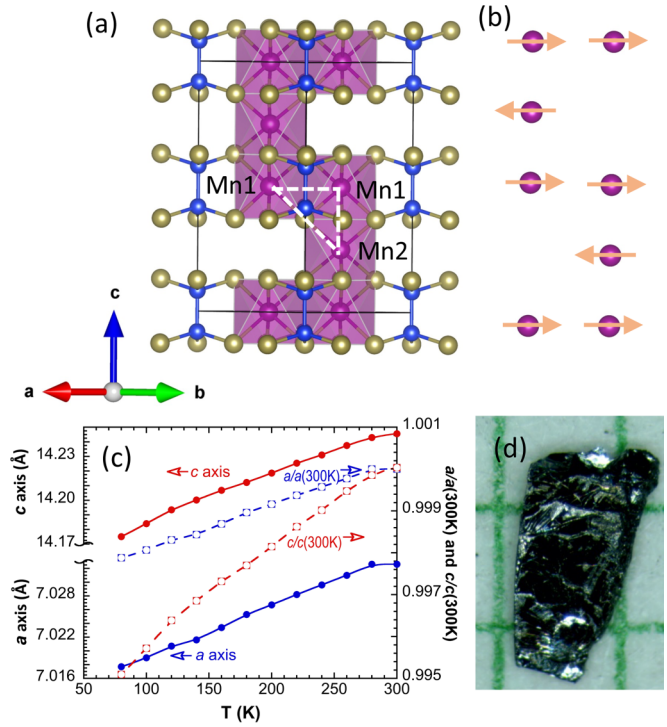

FIG. 1. Crystal structure. (a) The crystal structure highlighting the three-dimensional nature and bond distances for Mn1-Mn1 and Mn1-Mn2 marked by the white dashed lines. The third-nearest-neighbor interaction denoted by the diagonal dashed line proves consequential [23]. (b) The magnetic structure based on Ref. [23]. (c) The temperature dependence of the *a* and *c* axis, and the relative changes in the *a* and *c* axis against the values at 300 K (right scale). (d) A crystal sample showing the *ab* plane.

*gang.cao@colorado.edu

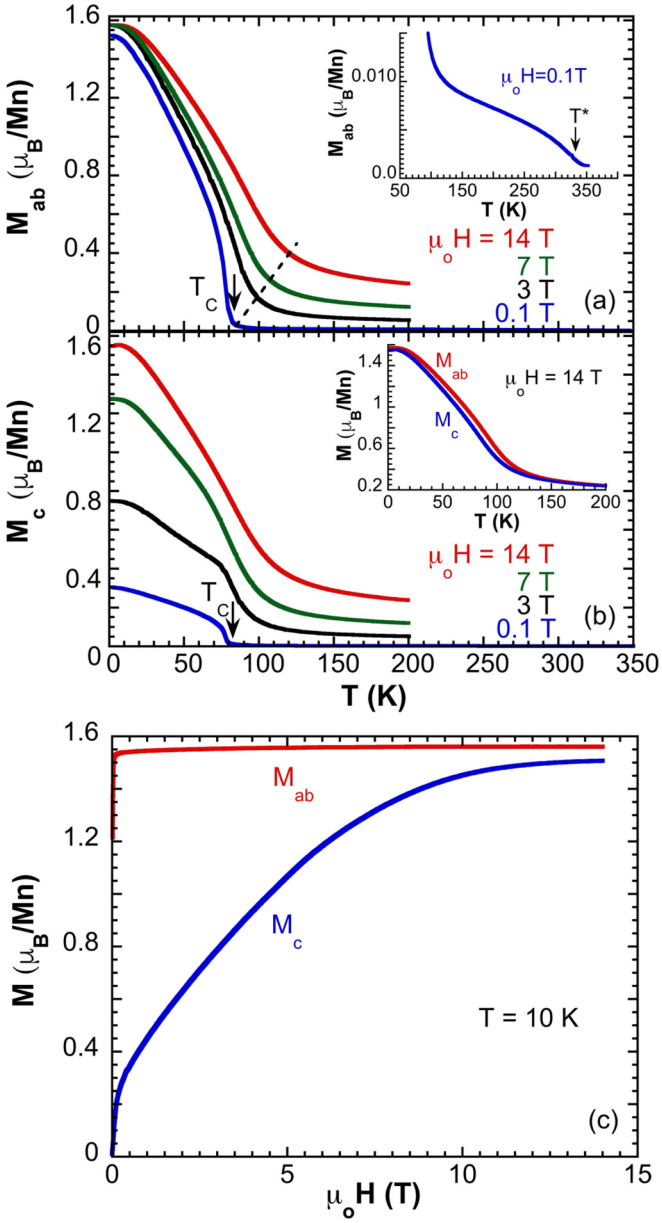

FIG. 2. Magnetic properties. The temperature dependence of (a) the *ab*-plane magnetization M_{ab} and (b) the *c*-axis magnetization M_c at various magnetic fields. Inset in (a): M_{ab} highlighting the correlated behavior at $T_C < T < T^*$. Inset in (b): $M_{ab}(T)$ and $M_c(T)$ at 14 T. (c) The isothermal magnetization M_{ab} and M_c at 10 K up to 14 T highlighting the anisotropy field. Note that M_{ab} saturates at $\mu_o H = 0.05$ T and M_c approaches M_s at $\mu_o H \geqslant 13$ T.

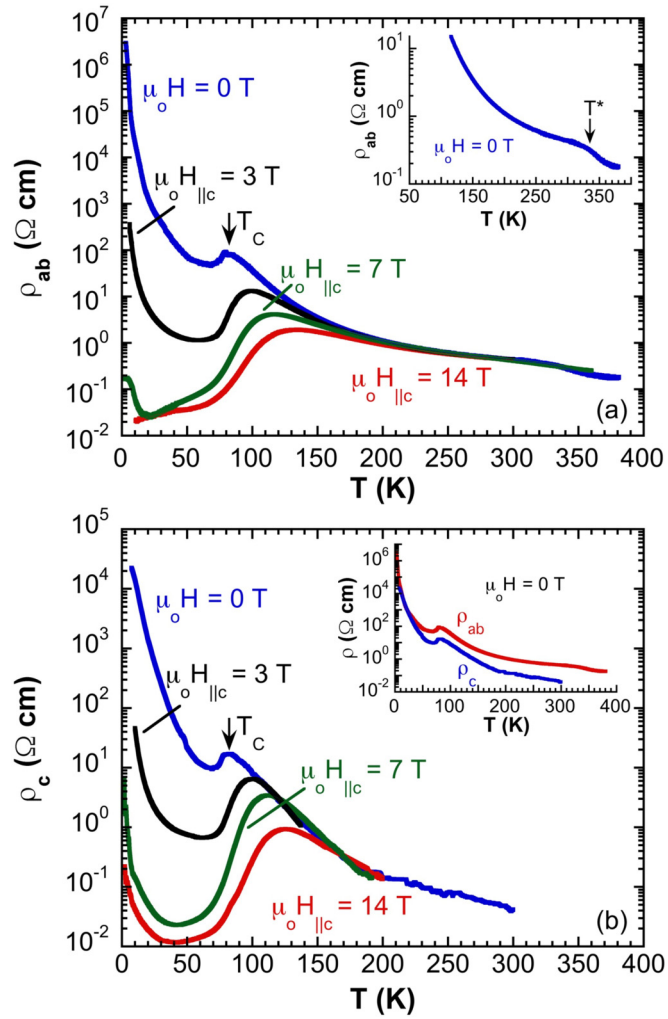

FIG. 3. Transport properties. The temperature dependence of (a) the *ab*-plane resistivity ρ_{ab} and (b) the *c*-axis resistivity ρ_c at various magnetic fields applied along the *c* axis. Note that ρ_{ab} drops by seven orders of magnitude or 99.999 99% at low temperatures and the T_{IM} shifts up to 130 K at 14 T. Inset in (a) ρ_{ab} highlighting anomaly corresponding to T^*. Inset in (b) showing $\rho_{ab} > \rho_c$.

Here we report a type of CMR in the stoichiometric chalcogenide $Mn_3Si_2Te_6$ that happens via avoiding a fully polarized magnetization, distinguishing from that observed previously in other materials. The three-dimensional $Mn_3Si_2Te_6$ with the $Mn^{2+}(3d^5)$ ions is a ferrimagnetic insulator with a ferrimagnetic Néel temperature $T_C = 78$ K [21–25]. This work reveals that the electrical resistivity drastically decreases by *seven orders of magnitude* or 99.999 99% ($1–10^{-7} = 1–0.000\,000\,1 = 0.999\,999\,9 = 99.999\,99\%$) at an applied magnetic field H above 9 T, inducing an insulator-metal transition T_{IM} at up to 130 K (note that MR is defined as $[\rho(H)–\rho(0)]/\rho(0)$). The reduction of resistivity is arguably among the largest values of CMR reported thus far. However, starkly different from CMR in other materials, the observed CMR *occurs only when H is applied along the magnetic hard axis*, the *c* axis, and is *absent when H is applied along the magnetic easy axis* which lies within the *ab* plane. The *ab*-plane magnetization readily and fully saturates at $\mu_o H \geqslant 0.05$ T with a saturation magnetization M_s of 1.56 μ_B/Mn, whereas the *c*-axis magnetization approaches this value only when $\mu_o H \geqslant 13$ T. Such an unusually strong magnetic anisotropy of 13 T is unexpected for the 3*d* ions with nominally quenched orbital momentum and negligible spin-orbit interactions (SOI). Moreover, our Hall effect data indicate a low carrier density ranging from $10^{23}/m^3$ to $10^{24}/m^3$. This type of CMR is intriguing and calls for urgent attention. (For experimental details see Ref. [26].)

$Mn_3Si_2Te_6$ has been known since 1981 [21,22]. It has drawn more attention in recent years because of its appar-

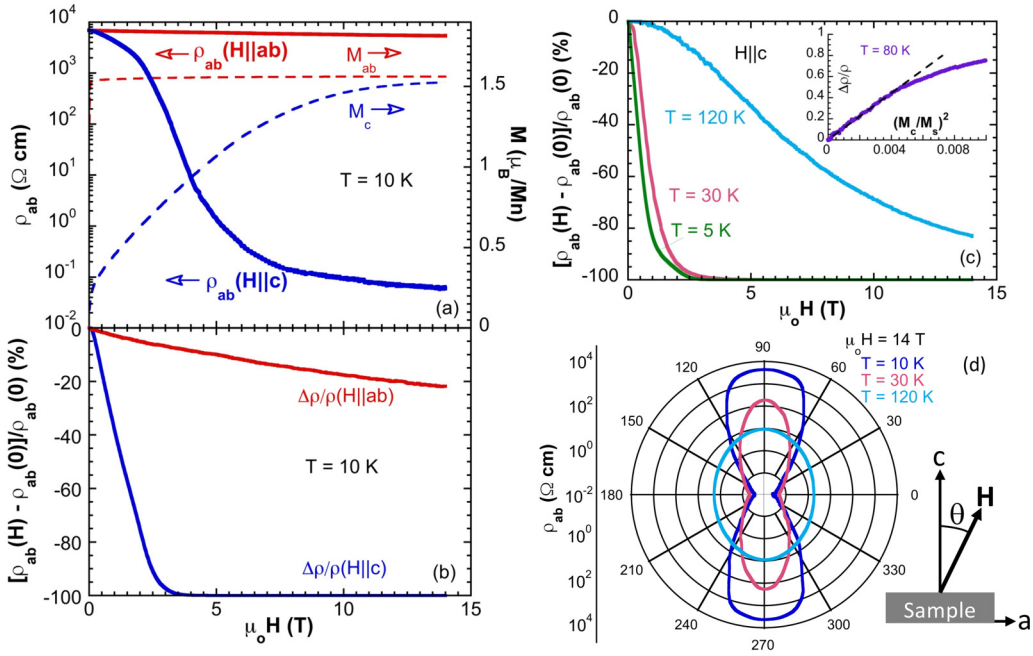

FIG. 4. Anisotropy and CMR below and above T_C. The magnetic field dependence at 10 K of (a) ρ_{ab} ($H||ab$) and ρ_{ab} ($H||c$) and M_{ab} and M_c (dashed lines, right scale), and (b) the corresponding $\Delta\rho_{ab}/\rho_{ab}(H||ab)$ and $\Delta\rho_{ab}/\rho_{ab}(H||c)$, where $\Delta\rho_{ab}/\rho_{ab} = [\rho_{ab}(H)-\rho_{ab}(0)]/\rho_{ab}(0)$. Note that $\Delta\rho_{ab}/\rho_{ab}(H||ab)$ is ~20% at $\mu_o H_{||ab} = 14$ T and $M_{ab} = M_s$ whereas $\Delta\rho_{ab}/\rho_{ab}(H||c)$ is already 97.50% at $\mu_o H_{||c} = 3$ T at which $M_c = 0.77\,\mu_B$/Mn $< 0.5 M_s$ and 99.999 99% at $\mu_o H_{||c} > 9$ T at which $M_c < M_s$. (c) The field dependence of $\Delta\rho_{ab}/\rho_{ab}(H||c)$ at 5, 30, and 120 K. Note that MR is still 85% at 120 K. Inset: The low-field scaling plot of $\Delta\rho_{ab}/\rho_{ab}(H||c) = C(M_c/M_s)^2$ for $\mu_o H_{||c} < 3.2$ T and 80 K $> T_C$, yielding $C = 105$ (dashed line). (d) The angular dependence of ρ_{ab} at 14 T and various temperatures. Inset: The angle θ measures the angle between H and the c axis.

ent relevance to van der Waals materials [23–25]. In this material, inherent frustration due to competing exchange interactions prevents a long-range order from setting in until the temperature is lowered to $T_C = 78$ K [23]. Results of diffuse magnetic scattering suggest short-range spin correlations existing well above T_C, possibly persisting up to 330 K [23]. Spin fluctuations thus may have important implications in the phenomena discussed below.

Crystal structure. $Mn_3Si_2Te_6$ adopts a trigonal structure having space group No. 163 [23]. Our single-crystal x-ray diffraction data as a function of temperature from 80 to 300 K are consistent with the reported results. In essence, $Mn_3Si_2Te_6$ consists of $MnTe_6$ octahedra edge sharing within the *ab* plane and face sharing along the *c* axis. Remarkably, the bond distance Mn1-Mn1 of two neighboring *edge-sharing* $MnTe_6$ octahedra in the *ab* plane is 4.0520 Å, whereas the bond distance Mn1-Mn2 of two neighboring *face-sharing* $MnTe_6$ octahedra along the *c* axis is much shorter, merely 3.5200 Å at 80 K, rendering more consequential exchange interactions between Mn1 and Mn2 [Fig. 1(a)]. The magnetic spins are ferromagnetically aligned within the *ab* plane and antiferromagnetically aligned along the *c* axis below T_C [Fig. 1(b)]. No magnetic canting is discerned [23]. The temperature dependence of the lattice parameters indicates that the *c* axis shrinks at a faster rate than the *a* axis, from 300 to 80 K [Fig. 1(c)]. No crystal structural change is observed. $Mn_3Si_2Te_6$ is clearly a robust three-dimensional lattice. The crystals are of 1–2 mm in size [Fig. 1(d)].

Magnetic properties. The magnetization M is measured as functions of magnetic field H and temperature T. The ferromagnetic transition $T_C = 78$ K broadens and shifts to higher temperatures as H increases [Figs. 2(a) and 2(b)]. Moreover, a well-defined magnetic anomaly also occurs at $T^* = 330$ K [inset in Fig. 2(a)], suggesting a short-range order due to inherent frustration [23]. Indeed, the temperature dependence of the *ab*-plane magnetization M_{ab} between T_C and T^* noticeably deviates from the Curie-Weiss law, indicating an absence of an anticipated paramagnetic state [inset in Fig. 2(a)].

The magnetic easy axis lies within the *ab* plane, where M_{ab} fully saturates at $\mu_o H \geqslant 0.05$ T and $T = 10$ K, resulting in $M_s = 1.56\,\mu_B$/Mn [Fig. 2(c)]. In contrast, the *c*-axis magnetization M_c approaches this value only when $\mu_o H \geqslant 13$ T. Note that M_c remains smaller than M_{ab}. Such a large anisotropy field of 13 T or $\sim 10^8$ A/m is unexpected for the 3*d* ions where both orbital momentum and SOI are nominally negligible. In general, magnetic anisotropy occurs because the crystal field stabilizes a preferred orbital that, via SOI, aligns the spin along a preferred crystallographic direction. However, the observed anisotropy field is surprisingly consistent with an *ab initio* calculation [23], predicting an anisotropy field of 13 T. The calculation suggests that the orbital moment is $0.037\,\mu_B$/Mn1 and $-0.048\,\mu_B$/Mn2, respectively [23]. Apparently, the orbital moment and SOI, however small, are surprisingly consequential in this material. Note that the observed $M_s(=1.56\,\mu_B/\text{Mn})$ is small for the $Mn^{2+}(3d^5)$ ion in which the Hund's rules dictate a high spin state $S = 5/2$ or possibly an intermediate spin state $S = 3/2$.

Transport properties. $Mn_3Si_2Te_6$ has an insulating ground state at ambient conditions [Fig. 3(a)]. The *ab*-plane resistivity

ρ_{ab} rises by 10^7 as T decreases from 380 to 3 K. A brief drop in ρ_{ab} below T_C is due to the reduction of spin scattering as the ferrimagnetic state sets in. ρ_{ab} rises again and rapidly below 60 K, reaching $3 \times 10^6\,\Omega\,\text{cm}$ at 3 K, and becomes unmeasurably too high below 3 K. The temperature dependence of ρ_{ab} below T_C strongly deviates from an activation law, ruling out thermal activation as an origin of the insulating state. In addition, ρ_{ab} exhibits a pronounced slope change near the magnetic anomaly $T^* = 330\,\text{K}$ [inset in Fig. 3(a)], which diminishes upon application of magnetic field, hinting at a suppressing of spin fluctuations.

Clearly, the resistivity is extremely sensitive to application of magnetic field. As demonstrated in Fig. 3(a), ρ_{ab} drastically decreases by *seven orders of magnitude* at low temperatures, leading to an insulator-metal transition T_{IM} when $H \parallel c$, e.g., $T_{\text{IM}} \approx 130\,\text{K}$ for $\mu_o H_{\parallel c} = 14\,\text{T}$.

The c-axis resistivity ρ_c responds to H in a similar but less dramatic manner [Fig. 3(b)]. However, unlike ρ_{ab}, ρ_c forms a pronounced valley between 30 and 60 K that reaches $10^{-2}\,\Omega\,\text{cm}$ before climbing back to a higher value. Note that $\rho_c < \rho_{ab}$ [inset in Fig. 3(b)], implying the importance of the shorter Mn1-Mn2 bond distance.

The resistivity is *extremely sensitive to the direction of* H in an unanticipated manner. As shown in Fig. 4(a), when $H \parallel ab$, ρ_{ab} drops by a mere 20% at 14 T (red solid lines). This is strikingly unusual because the magnetic easy axis lies within the ab plane, where M_{ab} readily and fully saturates at 0.05 T, reaching M_s (red dashed line). In sharp contrast, when $H \parallel c$, the magnetic hard axis, ρ_{ab} drops by 99.999 99% at $\mu_o H_{\parallel c} \geqslant 9\,\text{T}$ at which $M_c < M_s$ [Fig. 4(b)]. Note that ρ_{ab} already decreases by 97.50% at $\mu_o H_{\parallel c} = 3\,\text{T}$ at which $M_c = 0.77\,\mu_B/\text{Mn} < 0.5 M_s$ [blue dashed line in Fig. 4(a)]. Even at $T > T_C$, the absolute value of the negative MR remains large, e.g., 85% at 120 K [Fig. 4(c)]. In short, the CMR is *not coupled with the fully polarized magnetization* M_s and *emerges only when* M_s *is avoided*, which is at odds with CMR in other materials where magnetic polarization is essential.

The angular dependence of ρ_{ab} at 14 T at various temperatures provides more insight into this behavior. A polar plot generated based on the data is shown in Fig. 4(d). The angle θ measures the angle between H and the c axis, e.g., $\theta = 0^\circ$ for $H \parallel c$ and $\theta = 90^\circ$ for $H \parallel ab$ [inset in Fig. 4(d)]. ρ_{ab} as a function of θ forms elongated lobes pointing to $\theta = 90^\circ$ or 270° at 10 and 30 K. It visualizes the extraordinary anisotropy of ρ_{ab} that is smallest when H is parallel to the magnetic hard axis ($\theta = 0^\circ$ or 180°) and largest when H is parallel to the magnetic easy axis ($\theta = 90^\circ$ or 270°). The anisotropy weakens but is still visible at 120 K, well above T_C (=78 K), implying once again that the state above T_C involves substantial short-range correlations and is not a simple paramagnet.

This is also supported by the results of the Hall effect [Fig. 5(a)]. The Hall resistivity, ρ_{xy}, as a function of $H \parallel c$ exhibits a pronounced peak in the vicinity of 0.35 T for two representative temperatures below T_C, indicating the anticipated anomalous Hall effect (AHE). However, this peak persists, though broadened, above T_C, e.g., 120 K. This is unanticipated for a paramagnet where ρ_{xy} changes linearly with H. The linearity is eventually recovered at 200 K (lower inset in Fig. 5(a))

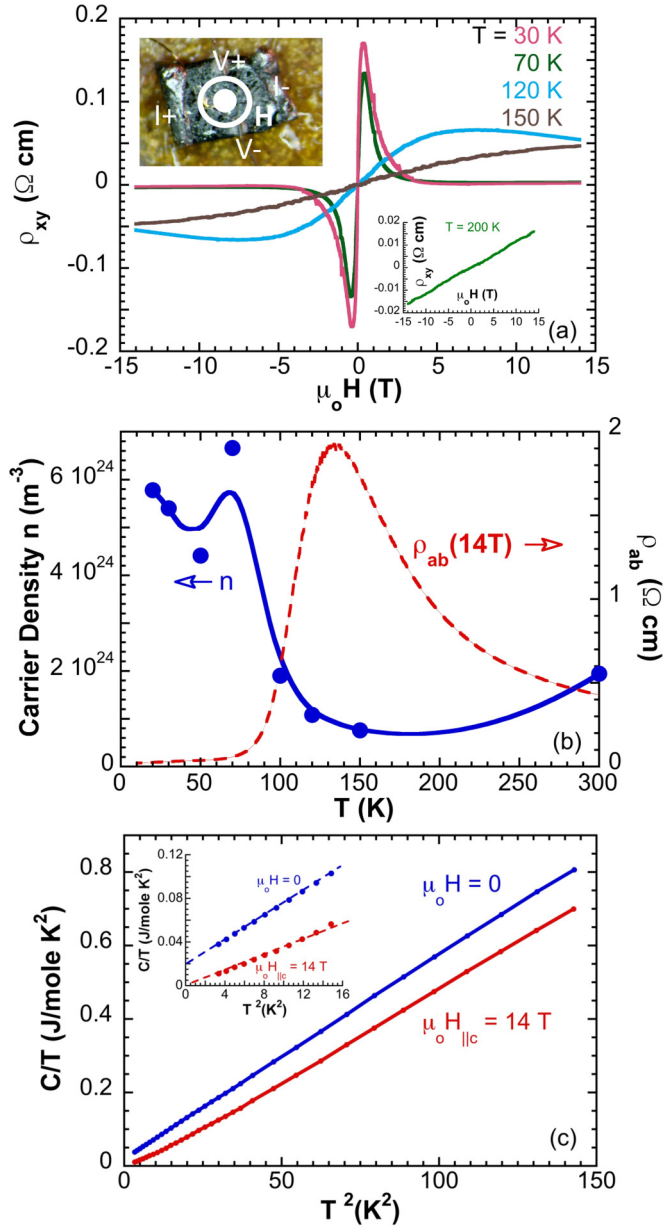

FIG. 5. Hall effect, carrier density, and heat capacity. (a) The field dependence of the Hall resistivity ρ_{xy} at representative temperatures. Note the AHE persisting up to $T > T_C$. Upper inset: The Hall sample with electrical leads and H pointing out of the page. Lower inset: $\rho_{xy}(H)$ at 200 K, showing the linear H dependence. (b) The temperature dependence of the carrier density n and ρ_{ab} at $\mu_o H_{\parallel c} = 14\,\text{T}$ (red dashed line, right scale). Note that n closely tracks ρ_{ab}. (c) The heat capacity $C(T)$ at zero field (blue) and $\mu_o H_{\parallel c} = 14\,\text{T}$ (red) plotted as $C(T)/T$ vs T^2. Note that the linear-T term due to the critical spin fluctuations is suppressed by H (see inset).

The carrier density n is retrieved from the linear portion of $\rho_{xy}(H)$ in a range of 11–14 T, well beyond the AHE peak, with subtraction of the residual AHE contribution. The assumption of a one-band structure might be overly simplistic, but it offers a useful estimate of n in this case. As shown in

Fig. 5(b), n, ranging from $10^{23}/\mathrm{m}^3$ to $10^{24}/\mathrm{m}^3$, closely tracks $\rho_{ab}(T)$ at 14 T (red dashed line). The sharp rise of n below 130 K indicates rapid delocalization of holes, leading to the metallic state.

The low n is consistent with the results from a low-field scaling relation of $[\rho(0)–\rho(H)]/\rho(0) = C(M/M_s)^2$ where C is a scaling constant proportional to $1/n^{2/3}$ [inset in Fig. 4(c)]. The value of C is reportedly smaller than 10 for hole-doped manganites [7], 15 for $Tl_2Mn_2O_7$ [17] and 50 for $Eu_5In_2Sb_6$ [19]. For $Mn_3Si_2Te_6$, $C = 105$, implying that the carrier density is indeed particularly low.

The heat capacity, $C(T)$, plotted as $C(T)/T$ vs T^2 [Fig. 5(c)] shows a large linear contribution of $C(T) \sim T$ with $C(T)/T = 23\,\mathrm{mJ/mole\,K}^2$ at $T = 0$ and $H = 0$. This is anticipated for a correlated metal with a high density of electronic states but unexpected for an insulator such as $Mn_3Si_2Te_6$. This linear term is suppressed by H (consistent with earlier reports [23]) and decreases to zero at $\mu_o H_{\|c} = 14\,\mathrm{T}$ when $Mn_3Si_2Te_6$ becomes a metal featuring the drastically enhanced n and conductivity below T_{IM} [Fig. 5(b)]. Clearly, the states that produce the linear term must lie within the magnetic sector and cannot be the conduction electrons.

The large linear term suggests gapless or critical magnetic fluctuations such as those arising from a coexisting or proximate critical phase, e.g., a spinon Luttinger liquid or a spinon-Fermi-surface quantum spin liquid [27–29]. Indeed, effective Luttinger liquids could emerge from the strong c-axis J_1 bonds, whereas spin liquids could occur due to sufficient frustration, which is evidenced by the suppressed T_C, the absence of Curie-Weiss behavior up to $T \approx 4T_C$, and the competing exchange interactions with $J_{1,2,3}$ showing $|J_3| > |J_2|$ [23]. Localized electrons could contribute a linear term susceptible to field suppression only via strong spin correlations leading again to gapless spinful excitations. Since the ab-plane spins are nearly fully polarized it is natural to assume that the critical magnetic fluctuations are associated with the c-axis spin degree of freedom. As such, the reduced density of states of the critical fluctuations [inset in Fig. 5(c)] corresponds to the slow spin polarization when $H \parallel c$ [Fig. 2(c)]. Note that these critical fluctuations are unrelated to critical-scaling curves near T_C [24] or to ferrimagnetic Goldstone modes.

The phenomena reported here cannot be explained by any existing models. However, the model developed for the ferromagnetic pyrochlore manganites [18] may provide a starting point for an eventual understanding. This model suggests that the ultralow-density carriers can form magnetic polarons dressed by mean-field ferromagnetic spin fluctuations in an intermediate temperature regime above T_C, and CMR emerges via suppressing the spin fluctuations [18]. In $Mn_3Si_2Te_6$, the presence of magnetic polarons is evidenced by the absence of the Curie-Weiss behavior and the persisting CMR and AHE above T_C. The magnetic polarons are now mostly dressed by the critical magnetic fluctuations associated with the c-axis spin degree of freedom. Suppressing the critical fluctuations can produce negative MR across the wide range of temperatures where the fluctuations are present. However, the key observation—that the CMR occurs only when fully polarized magnetization is avoided—is not an outcome of the model and is not captured by any other existing models. Clearly, the CMR reported here is fundamentally different from that in other materials, providing another direction for studying colossal magnetoresistance and its applications.

Acknowledgments. This work is supported by NSF via Grant No. DMR 1903888. G.C. is thankful to Peter Riseborough, Minhyea Lee, Dmitry Reznik, Dan Dessau, and Feng Ye for useful discussions.

[1] R. M. Kusters, J. Singleton, D. A. Keen, R. McGreevy, and W. Hayes, Magnetoresistance measurements on the magnetic semiconductor $Nd_{0.5}Pb_{0.5}MnO_3$, Phys. B (Amsterdam, Neth.) **155**, 362 (1989).

[2] R. von Helmolt, J. Wecker, B. Holzapfel, M. Schultz, and K. Samwer, Giant Negative Magnetoresistance in Perovskitelike $La_{2/3}Ba_{1/3}MnO_x$ Ferromagnetic Films, Phys. Rev. Lett. **71**, 2331 (1993).

[3] K. Chahara, T. Ohno, M. Kasai, and Y. Kozono, Magnetoresistance in magnetic manganese oxide with intrinsic antiferromagnetic spin structure, Appl. Phys. Lett. **63**, 1990 (1993).

[4] S. Jin, T. H. Tiefel, M. McCormack, R. A. Fastnacht, R. Ramesh, and L. H. Chen, Thousandfold change in resistivity in magnetoresistive La-Ca-Mn-O films, Science **264**, 413 (1994).

[5] Y. Tokura, A. Urushibara, Y. Moritomo, T. Arima, A. Asamitsu, G. Kido, and N. Furukawa, Giant magnetotransport phenomena in filling-controlled Kondo lattice system: $La_{1-x}Sr_xMnO_3$, J. Phys. Soc. Jpn **63**, 3931 (1994).

[6] A. Asamitsu, Y. Moritomo, Y. Tomioka, T. Arima, and Y. Tokura, A structural phase transition induced by an external magnetic field, Nature **373**, 407 (1995).

[7] A. Urushibara, Y. Moritomo, T. Arima, A. Asamitsu, G. Kido, and Y. Tokura, Insulator-metal transition and giant magnetoresistance in $La_{1-x}Sr_xMnO_3$, Phys. Rev. B **51**, 14103 (1995).

[8] A. J. Millis, B. I. Shraiman, and R. Mueller, Dynamic Jahn-Teller Effect and Colossal Magnetoresistance in $La_{1-x}Sr_xMnO_3$, Phys. Rev. Lett. **77**, 175 (1996).

[9] H. Röder, J. Zang, and A. R. Bishop, Lattice Effects in the Colossal-Magnetoresistance Manganites, Phys. Rev. Lett. **76**, 1356 (1996).

[10] A. P. Ramirez, Colossal magnetoresistance, J. Phys.: Condens. Matter **9**, 8171 (1997).

[11] J. M. D. Coey, M. Viret, and S. von Molnár, Mixed-valence manganites, Adv. Phys. **48**, 167 (1999).

[12] Y. Tokura, *Colossal Magnetoresistive Oxides* (Gordon and Breach, London, 2000).

[13] M. B. Salamon and M. Jaime, The physics of manganites: Structure and transport, Rev. Mod. Phys. **73**, 583 (2001).

[14] E. Dagotto, *Nanoscale Phase Separation and Colossal Magnetoresistance* (Springer, Berlin, 2002).

[15] E. Dagotto, T. Hotta, and A. Moreo, Colossal magnetoresistant materials: The key role of phase separation, Phys. Rep. **344**, 1 (2001).

[16] Y. Tokura, Critical features of colossal magnetoresistive manganites, Rep. Prog. Phys. **69**, 797 (2006).

[17] Y. Shimakawa, Y. Kubo, and T. Manako, Giant magnetoresistance in $Tl_2Mn_2O_7$ with the pyrochlore structure, Nature **379**, 53 (1996).

[18] P. Majumdar and P. Littlewood, Magnetoresistance in Mn Pyrochlore: Electrical Transport in a Low Carrier Density Ferromagnet, Phys. Rev. Lett. **81**, 1314 (1998).

[19] P. Rosa, Y. Xu, M. Rahn, J. Souza, S. Kushwaha, L. Veiga, A. Bombardi, S. Thomas, M. Janoschek, E. Bauer, M. Chan, Z. Wang, J. Thompson, N. Harrison, P. Pagliuso, A. Bernevig, and F. Ronning, Colossal magnetoresistance in a nonsymmorphic antiferromagnetic insulator, npj Quantum Mater. **5**, 52 (2020).

[20] D. T. Son and B. Z. Spivak, Chiral anomaly and classical negative magnetoresistance of Weyl metals, Phys. Rev. B **88**, 104412 (2013).

[21] R. Rimet, C. Schlenker, and H. Vincent, A new semiconducting ferrimagnet: A silicon manganese telluride, J. Magn. Magn. Mater. **25**, 7 (1981).

[22] H. Vincent, D. Leroux, D. Bijaoui, R. Rimet, and C. Schlenker, Crystal structure of $Mn_3Si_2Te_6$, J. Solid State Chem. **63**, 349 (1986).

[23] A. F. May, Y. Liu, S. Calder, D. S. Parker, T. Pandey, E. Cakmak, H. Cao, J. Yan, and M. A. McGuire, Magnetic order and interactions in ferrimagnetic $Mn_3Si_2Te_6$, Phys. Rev. B **95**, 174440 (2017).

[24] Y. Liu and C. Petrovic, Critical behavior and magnetocaloric effect in $Mn_3Si_2Te_6$, Phys. Rev. B **98**, 064423 (2018).

[25] L. M. Martinez, H. Iturriaga, R. Olmos, L. Shao, Y. Liu, T. T. Mai, C. Petrovic, A. R. H. Walker, and S. R. Singamaneni, Enhanced magnetization in proton irradiated $Mn_3Si_2Te_6$ van der Waals crystals, Appl. Phys. Lett. **116**, 172404 (2020).

[26] Single crystals of $Mn_3Si_2Te_6$ were grown using a flux method similar to that in Refs. [23,24]. The crystal structure was determined using a Bruker Quest ECO single-crystal x-ray diffractometer. Chemical analyses were performed using a combination of a Hitachi TM3030 Plus scanning electron microscope and an Oxford energy dispersive x-ray spectroscopy. The physical properties were measured using a Quantum Design Dynacool PPMS system and a MPMS-7 SQUID magnetometer.

[27] R. Mukhopadhyay, C. L. Kane, and T. C. Lubensky, Sliding Luttinger liquid phases, Phys. Rev. B **64**, 045120 (2001).

[28] P. A. Lee and N. Nagaosa, Gauge theory of the normal state of high-T_C superconductors, Phys. Rev. B **46**, 5621 (1992).

[29] See also discussion in G. Cao, H. Zheng, H. Zhao, Y. Ni, C. A. Pocs, Y. Zhang, F. Ye, C. Hoffmann, X. Wang, M. Lee *et al.*, Quantum liquid from strange frustration in the trimer magnet $Ba_4Ir_3O_{10}$, npj Quantum Mater. **5**, 26 (2020).